

# Automated Frame-by-Frame Endocardial Border Detection from Cardiac Magnetic Resonance Images for Quantitative Assessment of Left Ventricular Function: Validation and Clinical Feasibility

Cristiana Corsi, PhD,<sup>1\*</sup> Federico Veronesi, MS,<sup>1</sup> Claudio Lamberti, MS,<sup>1</sup> Dianna M.E. Bardo, MD,<sup>2</sup> Ernest B. Jamison, BS,<sup>2</sup> Roberto M. Lang, MD,<sup>2</sup> and Victor Mor-Avi, PhD<sup>2</sup>

**Purpose:** To develop a technique based on image noise distribution for automated endocardial border detection from cardiac magnetic resonance (CMR) images throughout the cardiac cycle, validate it, and test its clinical utility.

**Materials and Methods:** Images obtained in 36 patients were analyzed using custom software to obtain left ventricular (LV) volume throughout the cardiac cycle, end-systolic and end-diastolic LV volumes, and ejection fraction (EF). Validation against manually-traced endocardial boundaries included intertechnique comparisons of LV volumes, slice areas, and border positions. Then, the clinical feasibility of the dynamic automated analysis of LV function was tested in 14 patients with normal LV function, 12 patients with systolic dysfunction, and 10 patients with diastolic dysfunction.

**Results:** Analysis time for one cardiac cycle was <15 minutes. Intertechnique comparisons resulted in high correlation ( $r > 0.96$ ), small biases (volumes: -6 mL; EF: 4.6%) and narrow limits of agreement (volumes: 17.6 mL; EF: 9.2%). We found significant intergroup differences in multiple quantitative indices of systolic and diastolic function.

**Conclusion:** Fast, automated, dynamic detection of LV endocardial boundaries is feasible and allows accurate quantification of LV size and function, which is potentially clinically useful for objective assessment of systolic and diastolic dysfunction.

**Key Words:** ventricular function; magnetic resonance imaging; endocardial border detection; probabilistic level set; noise distribution

**J. Magn. Reson. Imaging 2009;29:560–568.**  
© 2009 Wiley-Liss, Inc.

CARDIAC MAGNETIC RESONANCE (CMR) is a noninvasive imaging modality with excellent spatial and con-

trast resolution that has become the standard reference in the assessment of left ventricular (LV) size and function (1,2), against which other techniques are frequently validated (3–12). However, this technique relies on the detection of endocardial boundaries, which requires frame-by-frame manual tracing on multiple slices, and is thus of limited value in clinical practice. Moreover, continuous measurement of LV volume requires slice-by-slice, phase-by-phase detection of the endocardial boundaries, which with the commercially available analysis software packages, based on the analysis of image intensity gradients, requires manual corrections in most patients and thus remains semiautomated at best, time consuming, and subjective. Thus, the dynamic nature of CMR imaging is largely unutilized in the clinical assessment of LV function, which is commonly reduced to visually identifying in a small number of slices the end-systolic (ES) and end-diastolic (ED) frames as those that depict the smallest and largest cross-sectional LV cavity areas, respectively. These frames are then traced slice-by-slice and used to obtain ES and ED volumes (ESV and EDV) and calculate the ejection fraction (EF). This practical solution can be challenging in patients with severely reduced systolic function, when volume changes are minimal, and inaccurate in hearts, wherein ventricular contraction is uneven and dyssynchronized so that minimum and maximum cross-sectional areas may appear in different slices at different times. Availability of a reliable technique for automated detection of the endocardial boundaries throughout the cardiac cycle would overcome this limitation and thus improve the accuracy of CMR quantification of LV size and function. Moreover, LV volume over time curves may provide clinically important information on LV dynamics (13), beyond the traditional ESV, EDV, and EF, and provide additional insight into LV contraction and relaxation properties.

Different techniques for endocardial contour detection from cardiac MR images have been described in the literature (14), including several reports on semiautomated and automated techniques (15–23), many of which were suitable for analysis of ED and ES phases

<sup>1</sup>Department of Electronics, Computer Science, and Systems, University of Bologna, Bologna, Italy.

<sup>2</sup>Medical Center, University of Chicago, Chicago, Illinois, USA.

\*Address reprint requests to: C.C., PhD, DEIS, University of Bologna, Viale Risorgimento 2, 40136 Bologna, Italy.  
E-mail: cristiana.corsi3@unibo.it

Received July 28, 2008; Accepted November 3, 2008.

DOI 10.1002/jmri.21681

Published online in Wiley InterScience (www.interscience.wiley.com).

only (15–17). Limitations of these approaches include a large number of manually segmented images required to build a model database (18–20) or to train the model (21–22), no continuous temporal segmentation (18), and computational complexity (23).

Accordingly, we sought to develop and test a new technique for fast, automated endocardial boundary detection throughout the cardiac cycle that would be suitable for clinical assessment of LV systolic and diastolic function. In contrast to the existing techniques, our approach does not rely on intensity gradients, but instead uses statistical distribution of gray levels to differentiate between the anatomic components in the image (18,19). If such tools become widely available, it is imperative for them to be rigorously validated and for their clinical utility to be tested in different groups of patients. Accordingly, our specific aims were: 1) to test the hypothesis that differences in noise patterns between myocardial tissue and the blood pool could be used as a basis for image segmentation and thus allow accurate automated detection of LV endocardial boundary; 2) to validate the automatically-detected endocardial boundaries as well as calculated cross-sectional LV areas and volumes against conventional methodology based on semiautomated tracing in patients with a wide range of EFs; and 3) to test the clinical utility of the automated approach by applying it to images obtained in patients with abnormal LV systolic and diastolic function and testing its ability to detect the expected intergroup differences.

## MATERIALS AND METHODS

### Study Design

Thirty-six patients referred for CMR evaluation of LV function were studied. Exclusion criteria were: inability to perform a 10- to 15-second breathhold, cardiac arrhythmias, prior sternotomy, pacemaker or defibrillator implantation, claustrophobia, and other known contraindications to CMR imaging. Written informed consent was obtained in all patients.

This study included two separate protocols. Protocol 1 was designed to test and validate the automated continuous measurements of LV size and function against the conventional methodology. Protocol 2 was designed to test the clinical utility and to determine whether indices of systolic and diastolic function extracted from volume–time curves are sensitive enough to differentiate between groups of patients with known and expected differences.

### CMR Imaging

CMR images were obtained using a 1.5T Intera Achieva scanner (Philips Medical Systems, Best, the Netherlands) with a phased-array cardiac coil. Electrocardiogram (ECG)-gated localizing spin-echo sequences were used to identify the LV long-axis and ensure the acquisition of anatomically correct short-axis views. Steady-state free precession dynamic gradient-echo mode was then used to acquire images during 10- to 15-second breathholds. The imaging parameters were as follows: echo time = 1 msec, repetition time = 3 msec, flip

angle = 60°, slice thickness = 8 mm with no gaps, field of view = 100 mm, scan matrix size = 256 × 256 pixels, and resolution varying from 1.25 × 1.25 mm<sup>2</sup> to 1.79 × 1.79 mm<sup>2</sup>. Cine-loops were obtained in 8 to 14 short-axis slices from the mitral annulus to LV apex with a temporal resolution of 30 frames per cardiac cycle.

### Slice Selection

LV slices were selected for analysis beginning with the highest basal slice where at least 50% of the LV cavity was surrounded by myocardial tissue, and ending with the lowest apical slice where the LV cavity was visualized during at least part of the cardiac cycle.

### Automated Technique

The automated technique was used in both protocols 1 and 2. CMR datasets were analyzed using custom software. For each frame, the 2D slices were stacked and LV endocardial boundaries were automatically detected throughout the cardiac cycle in all slices simultaneously to preserve spatial continuity. This was achieved by using a modified region-based level-set model, in which a priori knowledge of statistical distribution of gray levels in CMR data is embedded (20). The proposed method drives a surface evolution to achieve a maximum likelihood segmentation of the target with respect to the statistical distribution of image pixels. We considered the noise in CMR images to have a Rician probability density function that approaches a Gaussian function when pixel intensity is higher than the noise level. The probability density function and the functional values we defined and minimized to obtain maximally homogeneous 3D regions were previously described in detail (21). This model was implemented in the MATLAB 6.1 (MathWorks, Natick, MA, USA) environment, while the border detection algorithm was implemented in the C++ language to expedite processing.

The analysis software requires a definition of a single point within the LV cavity in a single slice at a single phase of the cardiac cycle as a seed for the initial spherical surface (Fig. 1a). This initialization is performed on the first frame only. The initial surface evolves until the region probability terms of the inside regions equal the terms of outside regions, up to the regularization of the surface. This process results in the detection of all homogeneous regions in the stack of image slices (Fig. 1b). Then, the undesired regions detected inside and outside the LV cavity, such as papillary muscles, cordae tendinae, and the right ventricular cavity, which are characterized by the same noise distribution, are automatically removed (Fig. 1c) using a simple algorithm based on the knowledge of the position of the initial seed point inside the LV cavity and the number of transitions between image components along each line of voxels. The use of this procedure consecutively for each frame resulted in the detection of LV endocardial boundaries throughout the cardiac cycle.

For each phase of the cardiac cycle, LV volume inside the detected surface was computed using the disk-area summation method. From each LV volume–time curve and its time-derivative, a series of indices of systolic

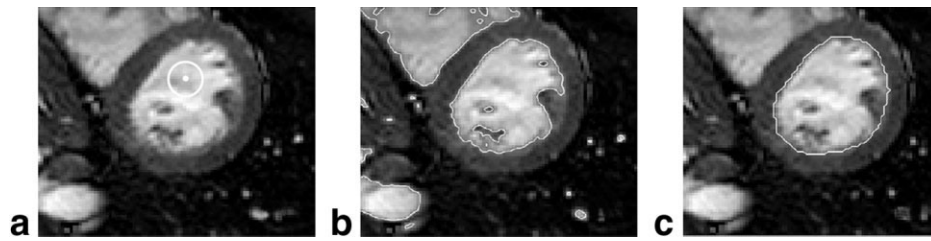


**Figure 1.** Example of automated endocardial border detection in one slice: (a) initial point selection; (b) results of the maximum likelihood segmentation; (c) final endocardial contour after the automatic deletion of the undesired detected regions outside and inside the LV chamber.

and diastolic LV function were calculated (Fig. 2), including EDV and ESV, which were obtained as the maximum and minimum volumes reached during in the cardiac cycle, respectively, and used to calculate EF as  $(EDV - ESV)/EDV \cdot 100$ . In addition, time from the R-wave to end-systole ( $t(ES)$ ), peak ejection rate (PER), and time to PER ( $t(PER)$ ) were computed. Indices of diastolic function included peak rapid and atrial filling rates (PRFR, PAFR) and their respective timings from end-systole ( $t(PRFR)$ ,  $t(PAFR)$ ) relative to the ECG R-wave, as well as rapid filling fraction (RFF) and atrial filling fraction (AFF). Ejection and filling rates were normalized by EDV.

To test the effects of the placement of a single seed point inside the LV cavity (which is the only user input in the analysis), the repeatability of volume measurements was tested in three randomly selected patients

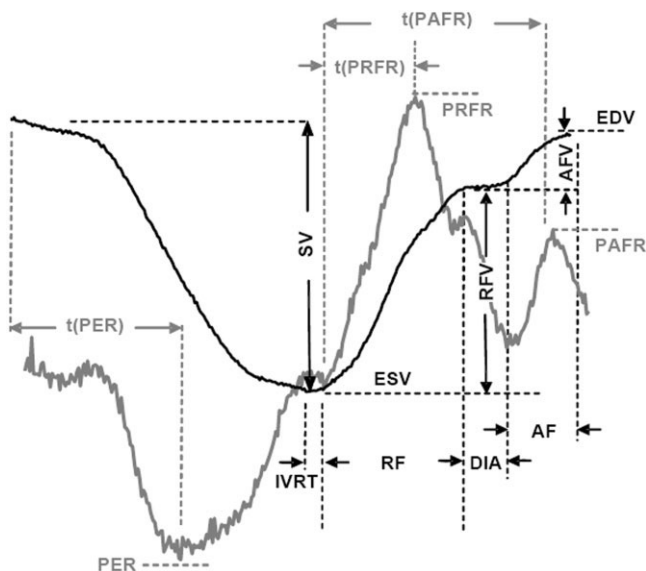


**Figure 2.** Schematic representation of LV volume time curve (solid black line) and its time derivative (solid gray line), and parameters of LV systolic and diastolic function extracted from these curves: ESV = end-systolic volume, EDV = end-diastolic volume, SV = stroke volume, RFF = rapid filling fraction, AFF = atrial filling fraction, PER = peak ejection rate,  $t(PER)$  = time to peak ejection rate, IVRT = isovolumic relaxation time, RF = rapid filling period, PRFR = peak rapid filling rate,  $t(PRFR)$  = time to peak rapid filling rate, DIA = diastasis period, AF = atrial filling period, PAFR = peak atrial filling rate, and  $t(PAFR)$  = time to peak atrial filling rate.

(total of 90 automatically detected endocardial boundaries). The operator, blinded to previous results repeated the analysis, and intermeasurement variability was computed as the absolute difference between the two measurements in percent of their mean.

### Reference Technique

The conventional technique was used only in protocol 1 for validation purposes. First, two to three midventricular slices were reviewed frame-by-frame by an experienced investigator to visually determine the smallest and largest LV cavity cross-sectional area. These phases of the cardiac cycle were used to measure ESV and EDV without having the complete volume time curves. Then, in every slice, LV endocardial contours were initially automatically detected frame-by-frame using commercial software (Philips ViewForum) with the papillary muscles included in the LV cavity. These contours were visually inspected and manually corrected in every slice of each frame, where such corrections were necessary for accurate border positioning. This resulted in LV cross-sectional area for each slice over time. Global LV volumes were computed throughout the cardiac cycle using the disk-area summation method, from which EDV and ESV were obtained as the maximum and minimum volumes and EF was calculated.

### Protocol 1

Protocol 1 comprised of 20 patients (age  $47 \pm 15$  years; 9 males) with a wide range of EFs. To validate the automated analysis of LV size and function, the following comparisons were made:

1. To determine the effects of the lack of temporal information on the reference values, ESV, EDV and EF obtained by visual determination of ES and ED were compared with values obtained from the volume-time curves.
2. To validate ESV, EDV, and EF values obtained by the automated technique as well as the automatically derived parameters of systolic and diastolic function (including  $t(ES)$ , PER,  $t(PER)$ , PRFR,  $t(PRFR)$ , PAFR, and  $t(PAFR)$ ), were compared with the reference values obtained from the conventional semiautomated reference volume-time curves.

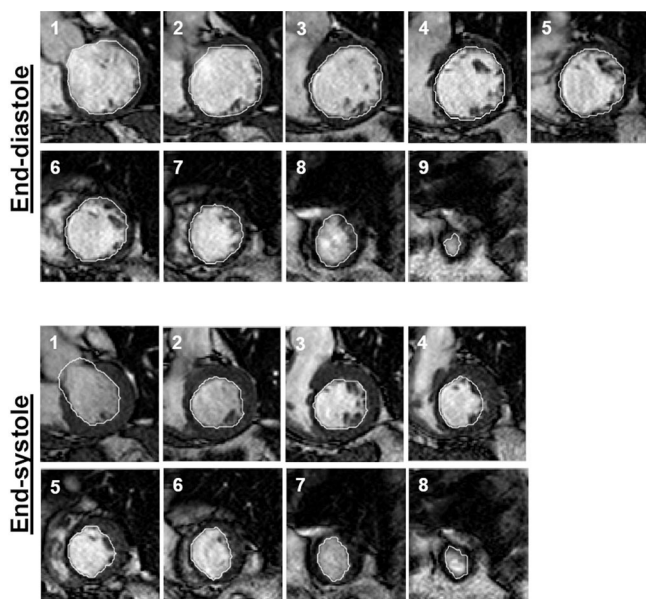


**Figure 3.** Example of the endocardial contours detected by the automated technique at end-diastole and end-systole, from the LV base (top left) to the apex (bottom right).

3. To validate the dynamic LV volume measurements, each time curve obtained with the automated technique was compared against the corresponding reference time curve.
4. To validate the position of the automatically detected boundaries, two indices were calculated for the ES and ED frames in each slice:  $\Delta r$ , the mean radial distance between the automatically detected and the traced endocardial contours, normalized by mean contour radius, and  $\Delta S$ , the percentage of the LV cavity area that did not overlap with the reference cavity area.

5. To identify the sources of error and assess the intertechnique agreement along the LV long-axis, normalized  $\Delta r$  and  $\Delta S$  were plotted against slice number for each patient. These variables were interpolated from LV base to apex (100 points, cubic spline) to compensate for the differences in the number of slices between patients, and then averaged over all patients.

### Protocol 2

Protocol 2 included three groups: 14 patients with normal LV function, 12 patients with systolic dysfunction due to dilated cardiomyopathy (DCM), and 10 patients with diastolic dysfunction secondary to LV hypertrophy (LVH). To test the clinical feasibility of the automated technique and evaluate the calculated indices of systolic and diastolic function in the clinical setting, the following comparisons were performed:

1. Indices of systolic function were compared between the 12 patients DCM (age,  $52 \pm 21$  years; 4 males;  $EF = 32 \pm 11\%$ ) and 14 normal subjects (age,  $49 \pm 15$  years; 9 males;  $EF = 62 \pm 11\%$ ).
2. Indices of diastolic function were compared between 10 patients with LVH (LV mass index =  $97 \pm 42$  g/m<sup>2</sup>; age,  $59 \pm 8$  years; 6 males) and 10 age-matched patients (LV mass index =  $56 \pm 16$  g/m<sup>2</sup>; age,  $57 \pm 9$  years; 9 males), selected from the normal group to take into account the well-known age-related differences in diastolic function.

### Statistical Analysis

In protocol 1, significance of differences in ESV, EDV, and EF computed using the reference technique with and without the complete temporal information was tested using paired, two-tailed *t*-test. Intertechnique comparisons of EDV, ESV, and EF included linear re-

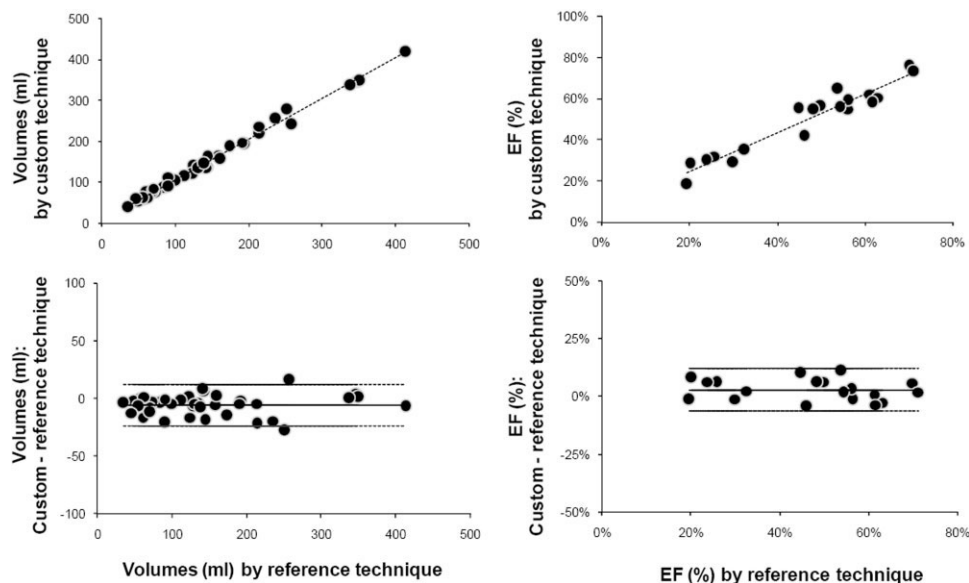


**Figure 4.** Linear regression (top) and Bland-Altman (bottom) analyses of EDV, ESV, and EF obtained using the conventional reference technique and the automated endocardial border detection based on analysis of statistical distribution of gray levels.

Table 1  
Parameters of LV Systolic and Diastolic Function Obtained in the 20 Patients in Protocol 1 Derived From the Automated Analysis Against Those Obtained Using the Reference Technique\*

	Reference technique	Automated analysis	r	Bias $\pm$ SD
t(ES) (%RR)	45.5 $\pm$ 9.4	44.8 $\pm$ 8.5	0.93	0.7 $\pm$ 3.4
PER (EDV/RR)	-11.6 $\pm$ 5.2	-11.3 $\pm$ 5.0	0.96	-0.3 $\pm$ 1.5
t(PER) (%RR)	19.5 $\pm$ 5.2	20.0 $\pm$ 5.7	0.88	-0.5 $\pm$ 2.7
PRFR (EDV/RR)	10.0 $\pm$ 4.7	10.1 $\pm$ 4.2	0.95	-0.1 $\pm$ 1.5
PAFR (EDV/RR)	7.6 $\pm$ 6.0	7.1 $\pm$ 5.4	0.98	0.5 $\pm$ 1.4
t(PRFR) (%RR)	62.0 $\pm$ 12.8	61.0 $\pm$ 12.5	0.98	1.0 $\pm$ 2.4
t(PAFR) (%RR)	90.0 $\pm$ 3.6	89.6 $\pm$ 3.4	0.89	0.4 $\pm$ 1.7

\*None of the indices were significantly different between the two techniques.

t(ES) = time to end-systole, PER = peak ejection rate, t(PER) = time to PER, PRFR = peak rapid filling rate, PAFR = peak atrial filling rate, t(PRFR) = time to PRFR, t(PAFR) = time to PAFR, EDV = end-diastolic volume, RR = ECG RR interval.

gression and Bland-Altman analyses. Additional indices of systolic and diastolic function were compared using paired, two-tailed *t*-test. Intertechnique percent discordance was computed for each pair of volume-time curves as the point-by-point sum of absolute differences between the values, normalized by the point-by-point sum of reference values. Intertechnique discordance in boundary position was estimated as the point-by-point sum of absolute differences between the radial distances from the LV cavity area center, normalized by the average contour radius. In protocol 2, indices of systolic function were compared between the group of patients with DCM and the normal controls using unpaired, two-tailed *t*-test. Indices of diastolic function were compared between the group of patients with LVH and the corresponding age-matched normal controls using paired, two-tailed *t*-test. *P* values <0.05 were considered significant.

## RESULTS

Measurements obtained using the commercial semiautomated technique were affected by the use of dynamic information on LV volumes. In 14 of the 20 patients studied in protocol 1 (70%), dynamic analysis resulted in differences of at least one frame in the determination of the timing of ES and/or ED compared to the conventional visual assessment. This resulted in small but nevertheless significant differences in the EDV, ESV, and EF measurements. EDV was underestimated by  $1.9 \pm 2.2$  mL ( $P = 0.007$ ), corresponding to  $1.1 \pm 1.4\%$  of the measured value, and ESV was overestimated by  $3.4 \pm 5.4$  mL ( $P = 0.036$ ), corresponding to  $2.3 \pm 1.9\%$  of the measured value. As a result, EF was underestimated by  $2.1 \pm 1.7\%$  ( $P < 0.0005$ ).

The automated analysis resulted in LV endocardial borders that were judged as accurate by an experienced cardiologist in all slices and all phases of the cardiac cycle in 35 of 36 patients (97%), by visualizing them superimposed on the MR images in both static and dynamic views. Importantly, in all patients, the entire boundary detection procedure, from the placement of a seed point in the LV cavity to having the final endocardial contours drawn throughout the cardiac cycle, required less than 15 minutes. In contrast, the conventional semiautomated technique required between 20

and 40 minutes depending on the number of slices and the extent of manual corrections necessary in each case. Of note, the intermeasurement variability in LV volume measurements was only  $0.7 \pm 0.4\%$ .

Figure 3 shows an example of ES and ED images with the automatically detected endocardial boundaries superimposed. In patients enrolled in protocol 1, the use of this technique resulted in high levels of agreement with the conventional semiautomated reference technique (Fig. 4), as reflected by high correlation coefficients, small biases, and narrow limits of agreement (volumes:  $y = 0.99x + 7.2$ ,  $r = 0.99$ , bias =  $-6.0$  mL [ $-3.8\%$  of mean reference value], SD = 8.9 mL; EF:  $y = 0.95x + 0.05$ ,  $r = 0.96$ , bias = 2.9%, SD = 4.6%). None of the measured indices of systolic and diastolic function were significantly different between the automated and the reference technique (Table 1).

Figure 5 shows an example of LV volume-time curves obtained in one patient by the conventional semiautomated technique and with the automated boundary detection. In the group of 20 patients, percent discordance averaged  $5.2 \pm 1.8\%$ , reflecting the close point-by-point agreement of the dynamic data obtained by the two techniques.

Figure 6 shows an example of ES and ED images with endocardial contours obtained in one patient using the

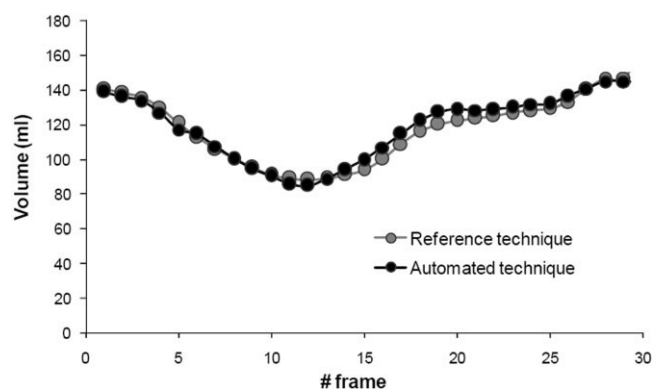
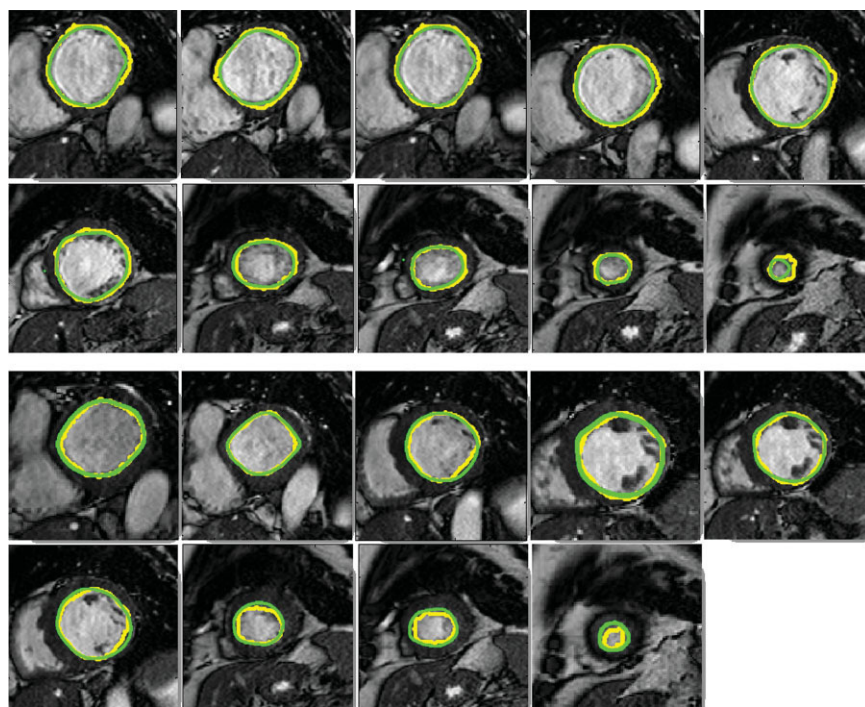


Figure 5. Example of LV volume time curves obtained in one patient by the conventional technique (Reference) and the automated endocardial border detection based on analysis of statistical distribution of gray levels. Calculated percent discordance in this example was 2.5%.

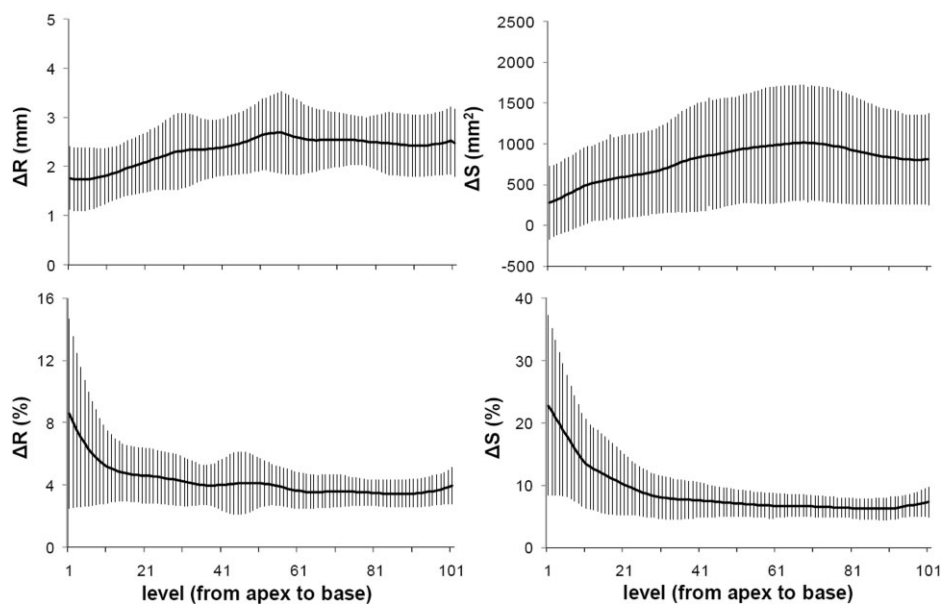


**Figure 6.** Example of the endocardial contours detected by the automated technique (yellow) and the semiautomatically traced contours (green) in one frame at end-systole and end-diastole, from LV base (top left) to the apex (bottom right). In this example, intertechnique discordance in boundary position was 4.8% of the average contour radius, resulting in 12.3% nonoverlapping cavity areas.

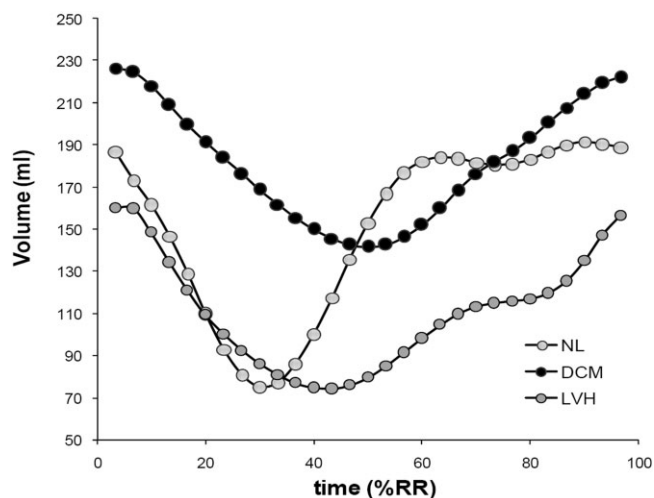
conventional semiautomated technique and the automated boundary detection, depicting the similarity between contours obtained using these two techniques. In the group of 20 patients, the intertechnique discordance in boundary position was  $2.4 \pm 0.3$  mm or  $4.2 \pm 1.0\%$  of the average contour radius (maximum  $\Delta r$  in individual patients:  $3.1 \pm 0.8$  mm), resulting in  $7.83 \pm 5.97$  cm<sup>2</sup> or  $9.2 \pm 3.2\%$  nonoverlapping cavity areas. The relative differences were found to be more pronounced near the apex (Fig. 7), due to the smaller size of the LV cavity in apical slices.

Figure 8 shows examples of volume–time curves obtained in three patients enrolled in protocol 2. As expected, compared to the curve obtained in a patient

with normal systolic function, the curve obtained in a patient with DCM is characterized by increased volumes and reduced peak-to-peak relative volume changes, i.e., reduced EF, as well as a decreased slope of the ejection phase, reflecting a decrease in PER. Table 2 presents the summary of indices of systolic LV function calculated in this group of patients in comparison with the normal group. Significant intergroup differences were noted for EDV, ESV, EF, PER,  $t(\text{ES})$ , and  $t(\text{PER})$ . In contrast, the curve obtained in a patient with LVH depicts the expected differences in LV relaxation pattern, compared to the normal subject, including a decreased slope of the rapid filling phase characteristic of impaired relaxation, as well as a relatively large pro-



**Figure 7.** Distance between the two boundaries ( $\Delta r$ , left) and difference between calculated cavity areas ( $\Delta S$ , right) at different levels of the left ventricle from base to apex (every 1% of the LV length) averaged in 20 patients (solid symbols represent mean values and error bars represent SD). Data shown both as absolute values (top) and in percent of the measured values (bottom).



**Figure 8.** Example of LV volume–time curves obtained in a patient with normal LV function (NL), a patient with dilated cardiomyopathy (DCM), and a patient with diastolic dysfunction secondary to LV hypertrophy (LVH), obtained using the automated endocardial border detection technique.

portion of late LV filling, which reflects the increased contribution of atrial contraction. Table 3 presents the summary of indices of diastolic function calculated in this group of patients and the subgroup of age-matched normal controls. Significant intergroup differences were found in all measured indices of diastolic function.

## DISCUSSION

The role of MRI in the diagnosis of heart disease has significantly expanded over the last few years, as multiple technological advances have resulted in faster image acquisition suitable for simultaneous dynamic imaging of the heart in multiple planes. Today, this modality provides multiplane dynamic images of the beating heart with excellent spatial resolution and temporal resolution of 30 phases per cardiac cycle, which is comparable to what has been for many years the standard frame rate in 2D echocardiography. The combina-

Table 3

Parameters of LV Diastolic Function Obtained in a Group of Patients With LV Hypertrophy and a Group of Age-Matched Normal Controls Obtained Using the Automated Technique

	NL (N = 10)	LVH (N = 10)
PRFR (EDV/RR)	2.3 ± 0.3	1.6 ± 0.4*
PAFR (EDV/RR)	0.9 ± 0.7	1.9 ± 0.9*
RFF (%)	78.2 ± 9.4	63.8 ± 12.4*
AFF (%)	21.8 ± 9.4	36.1 ± 12.3*
t(PRFR) (%RR)	54.3 ± 5.0	63.3 ± 5.5*
t(PAFR) (%RR)	88.3 ± 3.9	91.9 ± 1.8*

\* $P < 0.05$  by paired  $t$ -test between patients with LVH and their age-matched NL controls.

NL = normal controls, LVH = LV hypertrophy patients, PRFR = peak rapid filling rate, PAFR = peak atrial filling rate, RFF = rapid filling fraction, AFF = atrial filling fraction, t(PRFR) = time to PRFR, t(PAFR) = time to PAFR.

tion of these features places CMR imaging as the tentative “gold standard” for LV size and function, as reflected by multiple publications in which it was used as such to validate other noninvasive techniques (3–12).

However, the dynamic nature of CMR imaging is largely unutilized in the clinical assessment of LV function because of the lack of reliable algorithms for automated endocardial border detection. Only a few studies used the dynamic information because of the computational complexity, which hampered their online implementation (22). Our results demonstrated that the commonly employed alternative of measuring EDV and ESV only may indeed be inaccurate, since in the majority of patients it yielded different timing of ES when LV volume was measured frame-by-frame throughout the cardiac cycle. Of note, one might suggest that these small differences are not clinically significant and that they are below the error of most clinically used techniques. However, in certain situations, such as referral for cardiac resynchronization therapy, these small differences may determine the choice of therapy in individual patients, and therefore should not be underestimated.

Furthermore, this conventional methodology fails to provide important information on LV dynamics, such as the rates of rapid and atrial LV filling or percent filling at different phases of diastole, which have been shown as valuable indices of diastolic function. In clinical practice, the loss of this dynamic information, caused by the lack of algorithms suitable for automated endocardial border detection, is likely compensated for by additional testing, such as Doppler echocardiography, which readily provides this information. Thus, the development of improved algorithms suitable for accurate automated endocardial boundary detection from CMR images has the potential to not only improve the accuracy of the CMR evaluation of LV size and function, but also result in savings by eliminating duplicate tests.

Accordingly, we sought to develop a technique suitable for automated endocardial boundary detection from CMR images that would provide accurate dynamic information on LV volume throughout the cardiac cycle.

Table 2

Parameters of LV Systolic Function Obtained in a Group of Normal Subjects and a Group of Patients With Dilated Cardiomyopathy Obtained Using the Automated Technique

	NL (N = 14)	DCM (N = 12)
EDV (mL)	159 ± 47	244 ± 103*
ESV (mL)	63 ± 22	165 ± 93*
EF (%)	61 ± 5	36 ± 11*
t(ES) (%RR)	38.8 ± 5.0	50.6 ± 7.8*
PER (EDV/RR)	−2.7 ± 0.5	−1.3 ± 0.5*
t(PER) (%RR)	16.4 ± 3.6	23.6 ± 9.8*

\* $P < 0.05$  by  $t$ -test between patients with systolic dysfunction and NL controls.

NL = normal subjects, DCM = patients with dilated cardiomyopathy, EDV = end-diastolic volume, ESV = end-systolic volume, EF = ejection fraction, t(ES) = time to end-systole, PER = peak ejection rate, t(PER) = time to PER.

A majority of techniques described in the literature in this context are based on the use of image intensity gradients, and thus may not necessarily be ideally suited for CMR images, because gradients in these images may not be strong enough to allow accurate endocardial border detection and because the algorithms may be dependent on image quality and the specific pulse sequence used for imaging (23). There are different types of algorithms for boundary detection from CMR images, including approaches based on deformable models (24,25), active shape models (26,27), active appearance models (28,29), and expectation maximization method (30). However, these methods usually require extensive manual tracing for building the model database or for the definition of the training set, thus limiting their clinical application. In addition, the performance of these methods depends on how representative the training set is. We recently described a technique representing a case of the minimal partition problem that can be formulated and solved using the level set method (31,32). This model allows detecting objects with boundaries that are either not well defined by a gradient or are very smooth, thus limiting the usefulness of the classical active contour models. In addition, our model can be applied to a variety of images once the statistical distribution of noise in the image is known (21), with no need for a priori knowledge of the shape of the objects to be detected. Importantly, only one parameter needs to be set in the model and it allows choosing the maximum admissible boundary curvature: the regularization term that depends on this parameter and prevents the "rupture" of the interface (33).

The major goal of this study was to validate the use of this approach with CMR images against the standard semiautomated methodology in a group of patients with a wide range of LV function. The results of protocol 1 demonstrated that our technique indeed allows automated detection of LV endocardial boundaries without the need for manual corrections, which are very similar to boundaries manually drawn by an expert observer. The close agreement between boundary positions was demonstrated by the low intertechnique discordance in the average contour radius and the small nonoverlapping cavity areas. The increasing relative errors near the LV apex is not surprising in view of the decreasing contour radius and the relatively poor endocardial definition in apical short-axis slices as a result of partial volume artifacts that are more pronounced at this level of the ventricle. In addition, a small increase in the nonoverlapping cavity areas was noticed at the LV base due to the complex geometry of LV cavity in these slices.

Once validated against the conventional methodology in a group of patients with a wide range of ventricular performance, our approach was used to calculate a variety of indices of systolic and diastolic function in patients with known abnormalities in their ventricular function. Our results confirmed that this approach provides high-quality data suitable for analysis of a variety of quantitative indices of both systolic and diastolic function, which were found sensitive enough to detect the expected deviations from the normal patterns of LV contraction and filling.

One limitation of our technique is that its performance can be compromised in the presence of artifacts in the CMR images, such as off-frequency tuning artifacts, which can be recognized during visual interpretation. However, this limitation is not specific to our technique but would likely affect any automated image analysis technique. Accordingly, it is important to visually inspect the images to determine their suitability for automated analysis.

Although our approach requires significant computation time (up to 15 minutes per patient) for endocardial border detection, this limitation should be judged in the relevant context and thus compared with the time required to obtain the same information using conventional methodology, which in this study required up to three times longer to obtain the same dynamic data, and needless to say was significantly more involved than initializing a single point inside the LV cavity. Even EDV and ESV alone can rarely be obtained faster than obtaining the complete dynamic information using our automated technique. Moreover, analysis time of the automated technique is likely to decrease further as computational power of the available computer equipment continues to increase, while the time of the conventional technique, which is mainly based on user interaction, is not likely to change.

In summary, the results of this study demonstrated that the use of noise distribution rather than image intensity gradients for CMR image segmentation is feasible and allows fast, automated, frame-by-frame detection of the LV endocardial boundaries. The detected borders were close to those obtained by semiautomated tracing and resulted in high levels of agreement in cross-sectional LV cavity areas and calculated LV volumes throughout the cardiac cycle. Our results indicate that these dynamic volume data can be used clinically as a basis for quantitative evaluation of patients with either systolic or diastolic dysfunction.

## REFERENCES

1. Hundley WG, Meshack BM, Willett DL, et al. Comparison of quantitation of left ventricular volume, ejection fraction, and cardiac output in patients with atrial fibrillation by cine magnetic resonance imaging versus invasive measurements. *Am J Cardiol* 1996; 78:1119-1123.
2. Nagel E, Schneider U, Schalla S, et al. Magnetic resonance real-time imaging for the evaluation of left ventricular function. *J Cardiovasc Magn Reson* 2000;2:7-14.
3. Tadamura E, Kudoh T, Motooka M, et al. Assessment of regional and global left ventricular function by reinjection T1-201 and rest Tc-99m sestamibi ECG-gated SPECT: comparison with three-dimensional magnetic resonance imaging. *J Am Coll Cardiol* 1999; 33:991-997.
4. Bax JJ, Lamb H, Dibbets P, et al. Comparison of gated single-photon emission computed tomography with magnetic resonance imaging for evaluation of left ventricular function in ischemic cardiomyopathy. *Am J Cardiol* 2000;86:1299-1305.
5. Poutanen T, Ikonen A, Jokinen E, Vainio P, Tikanoja T. Transthoracic three-dimensional echocardiography is as good as magnetic resonance imaging in measuring dynamic changes in left ventricular volume during the heart cycle in children. *Eur J Echocardiogr* 2001;2:31-39.
6. Thiele H, Paetsch I, Schnackenburg B, et al. Improved accuracy of quantitative assessment of left ventricular volume and ejection fraction by geometric models with steady-state free precession. *J Cardiovasc Magn Reson* 2002;4:327-339.

7. Malm S, Frigstad S, Sagberg E, Larsson H, Skjaerpe T. Accurate and reproducible measurement of left ventricular volume and ejection fraction by contrast echocardiography: a comparison with magnetic resonance imaging. *J Am Coll Cardiol* 2004;44:1030–1035.
8. Hoffmann R, von BS, ten CF, et al. Assessment of systolic left ventricular function: a multi-centre comparison of cineventriculography, cardiac magnetic resonance imaging, unenhanced and contrast-enhanced echocardiography. *Eur Heart J* 2005;26:607–616.
9. Dewey M, Muller M, Eddicks S, et al. Evaluation of global and regional left ventricular function with 16-slice computed tomography, biplane cineventriculography, and two-dimensional transthoracic echocardiography: comparison with magnetic resonance imaging. *J Am Coll Cardiol* 2006;48:2034–2044.
10. Sugeng L, Mor-Avi V, Weinert L, et al. Quantitative assessment of left ventricular size and function: side-by-side comparison of real-time three-dimensional echocardiography and computed tomography with magnetic resonance reference. *Circulation* 2006;114:654–661.
11. Jenkins C, Bricknell K, Chan J, Hanekom L, Marwick TH. Comparison of two- and three-dimensional echocardiography with sequential magnetic resonance imaging for evaluating left ventricular volume and ejection fraction over time in patients with healed myocardial infarction. *Am J Cardiol* 2007;99:300–306.
12. Schlosser T, Mohrs OK, Magedanz A, Voigtlander T, Schmermund A, Barkhausen J. Assessment of left ventricular function and mass in patients undergoing computed tomography (CT) coronary angiography using 64-detector-row CT: comparison to magnetic resonance imaging. *Acta Radiol* 2007;48:30–35.
13. Corsi C, Lang RM, Veronesi F, et al. Volumetric quantification of global and regional left ventricular function from real-time three-dimensional echocardiographic images. *Circulation* 2005;112:1161–1170.
14. Frangi AF, Niessen WJ, Viergever MA. Three-dimensional modeling for functional analysis of cardiac images: a review. *IEEE Trans Med Imaging* 2001;20:2–25.
15. Stegmann MB, Pedersen D. Bi-temporal 3D active appearance models with applications to unsupervised ejection fraction estimation. *Medical Imaging 2005: Image Processing*, Fitzpatrick JM, Reinhardt JM, eds. Proceedings of the SPIE, 2005;5747:336–350.
16. Mitchell SC, Bosch JG, Lelieveldt BP, van der Geest RJ, Reiber JH, Sonka M. 3-D active appearance models: segmentation of cardiac MR and ultrasound images. *IEEE Trans Med Imaging* 2002;21:1167–1178.
17. Uzumcu M, van der Geest RJ, Sonka M, Lamb HJ, Reiber JH, Lelieveldt BP. Multiview active appearance models for simultaneous segmentation of cardiac 2- and 4-chamber long-axis magnetic resonance images. *Invest Radiol* 2005;40:195–203.
18. Gudbjartsson H, Patz S. The Rician distribution of noisy MRI data. *Magn Reson Med* 1995;34:910–914.
19. Gravel P, Beaudoin G, De Guise JA. A method for modeling noise in medical images. *IEEE Trans Med Imaging* 2004;23:1221–1232.
20. Corsi C, Veronesi F, Lamberti C, Mor-Avi V. Improved automated quantification of left ventricular size and function from cardiac magnetic resonance images. *Comput Cardiol* 2006;33:53–56.
21. Sarti A, Corsi C, Mazzini E, Lamberti C. Maximum likelihood segmentation of ultrasound images with Rayleigh distribution. *IEEE Trans Ultrason Ferroelectr Freq Control* 2005;52:947–960.
22. Uzumcu M, van der Geest RJ, Swingen C, Reiber JH, Lelieveldt BP. Time continuous tracking and segmentation of cardiovascular magnetic resonance images using multidimensional dynamic programming. *Invest Radiol* 2006;41:52–62.
23. Angelie E, de Koning PJ, Danilouchkine MG, et al. Optimizing the automatic segmentation of the left ventricle in magnetic resonance images. *Med Phys* 2005;32:369–375.
24. McInerney T, Terzopoulos D. Deformable models in medical image analysis: a survey. *Med Image Anal* 1996;1:91–108.
25. Lotjonen J, Reissman PJ, Magnin IE, Katila T. Model extraction from magnetic resonance volume data using the deformable pyramid. *Med Image Anal* 1999;3:387–406.
26. van Assen HC, Danilouchkine MG, Frangi AF, et al. SPASM: a 3D-ASM for segmentation of sparse and arbitrarily oriented cardiac MRI data. *Med Image Anal* 2006;10:286–303.
27. Lotjonen J, Kivisto S, Koikkalainen J, Smutek D, Lauerma K. Statistical shape model of atria, ventricles and epicardium from short- and long-axis MR images. *Med Image Anal* 2004;8:371–386.
28. van der Geest RJ, Lelieveldt BP, Angelie E, et al. Evaluation of a new method for automated detection of left ventricular boundaries in time series of magnetic resonance images using an active appearance motion model. *J Cardiovasc Magn Reson* 2004;6:609–617.
29. Angelie E, Oost ER, Hendriksen D, Lelieveldt BP, van der Geest RJ, Reiber JH. Automated contour detection in cardiac MRI using active appearance models: the effect of the composition of the training set. *Invest Radiol* 2007;42:697–703.
30. Lorenzo-Valdes M, Sanchez-Ortiz GI, Mohiaddin R, Rueckert D. Segmentation of 4D cardiac MR images using a probabilistic atlas and the EM algorithm. *Med Image Comput Comput Assist Interv Int Conf Med Image Comput Comput Assist Interv* 2003;2878:440–450.
31. Osher S, Sethian JA. Fronts propagating with curvature-dependent speed—algorithms based on Hamilton-Jacobi formulations. *J Comput Physics* 1988;79:12–49.
32. Sethian JA. *Level set methods and fast marching methods*. Cambridge, UK: Cambridge University Press; 1999.
33. Mumford D, Shah J. Optimal approximation by piecewise smooth functions and associated variational problems. *Pure Appl Math* 1989;42:577–585.